AIP | Applied Physics Letters

Nanoscale-resolved chemical identification of thin organic films using infrared near-field spectroscopy and standard Fourier transform infrared references

Stefan Mastel, Alexander A. Govyadinov, Thales V. A. G. de Oliveira, Iban Amenabar, and Rainer Hillenbrand

Citation: Applied Physics Letters **106**, 023113 (2015); doi: 10.1063/1.4905507
View online: http://dx.doi.org/10.1063/1.4905507
View Table of Contents: http://scitation.aip.org/content/aip/journal/apl/106/2?ver=pdfcov
Published by the AIP Publishing

Nanoscale-resolved chemical identification of thin organic films using infrared near-field spectroscopy and standard Fourier transform infrared references

Stefan Mastel,[1] Alexander A. Govyadinov,[1] Thales V. A. G. de Oliveira,[1] Iban Amenabar,[1] and Rainer Hillenbrand[2,3,a)]
[1]*CIC NanoGUNE, 20018 Donostia-San Sebastán, Spain*
[2]*CIC NanoGUNE and EHU/UPV, 20018 Donostia-San Sebastián, Spain*
[3]*IKERBASQUE, Basque Foundation for Science, 48011 Bilbao, Spain*

(Received 6 November 2014; accepted 21 December 2014; published online 13 January 2015)

We establish a solid basis for the interpretation of infrared near-field spectra of thin organic films on highly reflective substrates and provide guidelines for their straightforward comparison to standard far-field Fourier transform infrared (FTIR) spectra. Particularly, we study the spectral behavior of near-field absorption and near-field phase, both quantities signifying the presence of a molecular resonance. We demonstrate that the near-field phase spectra only weakly depend on the film thickness and can be used for an approximate comparison with grazing incidence FTIR (GI-FTIR) spectra. In contrast, the near-field absorption spectra can be compared more precisely with far-field spectra: for ultrathin films they match well GI-FTIR spectra, while for thick films a good agreement with standard transmission FTIR spectra is found. Our results are based on experimental data obtained by nanoscale FTIR (nano-FTIR) spectroscopy and supported by a comprehensive theoretical analysis. © *2015 AIP Publishing LLC*. [http://dx.doi.org/10.1063/1.4905507]

Scattering-type scanning near-field optical microscopy (s-SNOM)[1] and nanoscale Fourier transform infrared spectroscopy (nano-FTIR)[2–4] are versatile near-field techniques for nanoscale chemical identification. In s-SNOM, nanoscale-resolved infrared images are obtained by interferometric recording of the infrared light scattered at an atomic force microscope (AFM) tip.[1] Probing of the sample's local infrared response, including molecular vibrational absorption, is based on the near-field interaction between tip apex and sample surface, resulting in a modification of the scattered field. By sequential imaging of the sample at different wavelengths, infrared near-field spectra can be obtained.[5–15] Alternatively, in nano-FTIR spectroscopy, the tip is illuminated by broadband infrared radiation and the interferometer is used as an asymmetric[16] Fourier transform spectrometer, yielding infrared near-field spectra with a spatial resolution of about 20 nm.[3,4,17,18]

Importantly, the interferometric detection yields both near-field amplitude s and phase φ. It has been found that the near-field phase spectra, $\varphi(\omega)$, relate to the absorptive properties of molecular samples.[7,8,19,20] However, a quantitative comparison with transmission far-field FTIR spectroscopy[21] reveals that the peak positions do not necessarily coincide.[17,22] Instead, for thick organic films, the peak positions of FTIR absorbance spectra match well with that of the so-called near-field or nano-FTIR absorption spectra $a(\omega) = s(\omega)\sin(\varphi(\omega))$.[4,12,23] This finding promises a convenient identification of nanomaterials in the mid-IR fingerprint region by simply comparing nano-FTIR absorption spectra with standard FTIR spectra from databases. On the other hand, recent studies indicate that nano-FTIR absorption spectra of thin samples (thickness $d <$ tip apex radius R_t) on highly reflective substrates are blueshifted, while matching well with grazing-incidence FTIR (GI-FTIR) spectra.[17] Here, we address this issue with an experimental and theoretical study of near- and far-field infrared spectra of thin organic films of varying thickness on highly reflective substrates. We provide basic physical insights and practical guidelines for nanoscale material characterization based on direct comparison of near-field spectra with standard far-field references.

As sample we used spin-coated Poly(methyl methacrylate) (PMMA) films on silicon, as PMMA exhibits well-defined molecular vibrational resonances.[4] As typical in s-SNOM and nano-FTIR, a silicon substrate is used to enhance the near-field signal of the organic film (substrate-enhanced near-field spectroscopy).[24,25]

For the experiments, we used a commercial s-SNOM and nano-FTIR setup (Neaspec GmbH, Germany), illustrated in Figure 1(a). A gold-coated standard AFM tip oscillating vertically at frequency $\Omega \approx 120$ kHz was employed as near-field probe. The tip was illuminated by either a tunable quantum cascade laser (QCL, Daylight Solutions, Inc., USA) or a broadband mid-infrared laser continuum.[4] For effective background suppression, the tip-scattered signal was demodulated at higher harmonics $n\Omega$ of the cantilever oscillation frequency, yielding near-field amplitude and phase signals, s_n and φ_n, respectively.[1] Throughout this work $n = 3$.

By using the QCL and operating the interferometer in synthetic optical holography (SOH) mode[26,27] two sets of single-wavelength near-field amplitude s_3 and phase φ_3 images (Fig. 1(d)) were recorded simultaneously to topography (Fig. 1(c)). The images recorded on resonance with the C = O stretching bond of the PMMA molecules (1731 cm^{-1}) verify both the nanoscale spatial resolution of the setup and

a)Author to whom correspondence should be addressed. Electronic mail: r.hillenbrand@nanogune.eu

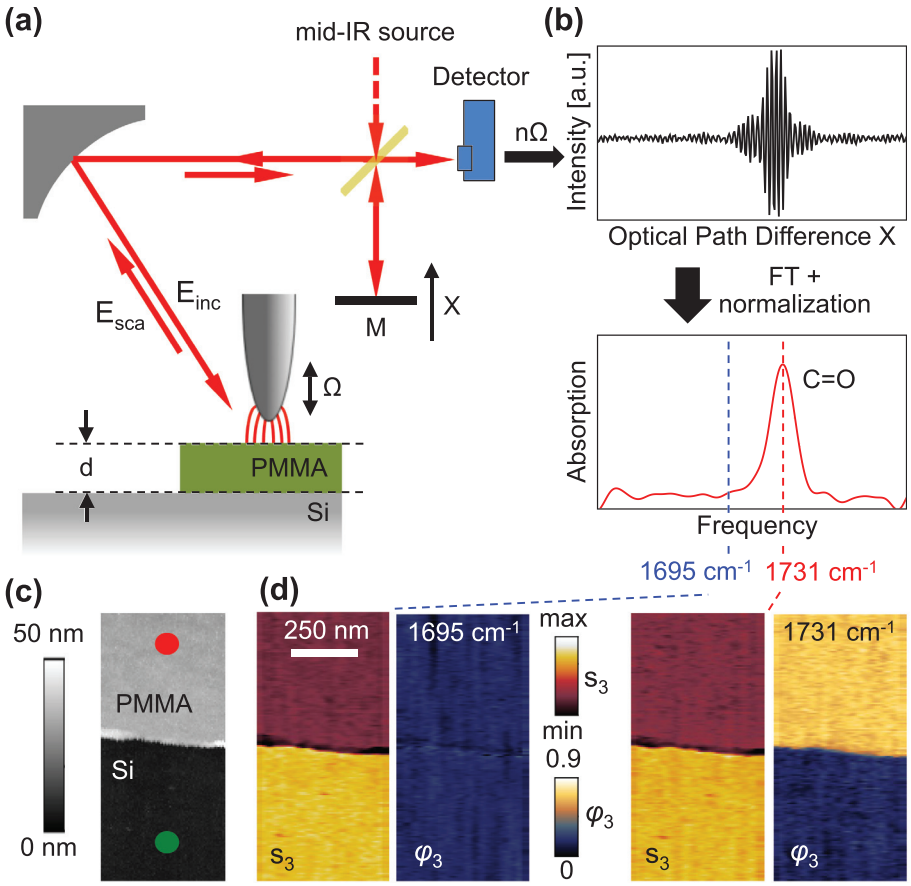

FIG. 1. Near-field imaging and spectroscopy of thin polymer films. (a) s-SNOM and nano-FTIR setup. (b) Near-field interferogram and the corresponding near-field absorption spectrum. (c) Topography of a 31 nm PMMA film on Si. Red and green dots mark positions where PMMA and reference nano-FTIR spectra were taken. (d) Near-field amplitude s_3 and phase φ_3 images at 1695 cm^{-1} and 1731 cm^{-1}.

the expected phase contrast (revealing absorption) relative to the non-absorbing silicon substrate.[7] Off-resonance (1695 cm^{-1}), the vanishing phase contrast indicates the absence of molecular absorption.

For nano-FTIR spectroscopy, the reference mirror M in Figure 1(a) is translated at a fixed sample position to acquire an interferogram of the tip-scattered mid-infrared laser continuum (Fig. 1(b)). A complex Fourier transformation yields near-field amplitude $s_3(\omega)$ and phase $\varphi_3(\omega)$ spectra. Analogous to far-field FTIR spectroscopy, the nano-FTIR data of the PMMA film are normalized to a non-absorbing reference, yielding the PMMA spectrum (near-field contrast) $\eta_3(\omega) = s_3 \exp(i\varphi_3) = (s_{3,\mathrm{PMMA}}/s_{3,\mathrm{ref}}) \exp(i(\varphi_{3,\mathrm{PMMA}} - \varphi_{3,\mathrm{ref}}))$. The reference spectra $s_{3,\mathrm{ref}}$ and $\varphi_{3,\mathrm{ref}}$ were recorded on the silicon substrate.

Figure 2 shows the measured nano-FTIR spectra for PMMA films of different thicknesses d and compares them to far-field FTIR spectra. All far-field spectra display the absorbance, that is, $A_t = -\log(I_t/I_0)$ for FTIR and $A_r = -\log(R/R_0)$ for GI-FTIR spectroscopy. I_t is the power transmitted through the sample, and I_0 is the incident power. R is the power reflected from the film on a substrate, and R_0 is the power reflected at the bare substrate. All near-field amplitude s_3 spectra (Fig. 2(a)) reveal a dispersive behavior around the C = O resonance, whereas the phase φ_3 spectra (Fig. 2(b)) exhibit an absorption-like peak at 1738 cm^{-1}. Both observations are typical for the spectral near-field response of an organic material.[7,8,25] With decreasing film thickness, the amplitude values increase, which can be explained by the enhanced near-field interaction between tip and silicon substrate.[24,25,28] Simultaneously, the peak height of the phase decreases, which can be attributed to the reduced amount of the probed PMMA.[25] Importantly, we observe that the peak position in all phase spectra is nearly independent of the film thickness, while being blueshifted by about 3 cm^{-1} compared to the GI-FTIR spectrum (Fig. 2(d)). The peak position of the near-field absorption spectra a_3 (Fig. 2(c)), in contrast, shifts to lower frequencies when the film thickness increases. Interestingly, the peak position of the thick-film near-field absorption spectrum ($d = 174$ nm) matches well the far-field FTIR peak of bulk PMMA (dashed black curve, Fig. 2(d)), while the near-field absorption spectrum of the thinnest film ($d = 10$ nm) matches well the GI-FTIR spectrum (dashed red curve, Fig. 2(d)).

To understand the experimental results, we performed a theoretical comparison of far- and near-field spectra based on the film's dielectric permittivity $\epsilon = \epsilon' + i\epsilon''$. The absorbance spectra, A_t, of thick films measured by transmission FTIR spectroscopy yield the absorption coefficient $\kappa = \mathrm{Im}(\sqrt{\epsilon}) = \mathrm{Im}(\sqrt{\epsilon' + i\epsilon''})$.[21,29] For weak oscillators with $\epsilon'' < \epsilon'$, we obtain

$$A_t \propto \kappa \approx \frac{1}{2\sqrt{\epsilon'}}\epsilon''. \quad (1)$$

We find that $\kappa(\omega)$ (black curve, Fig. 3(a)) is slightly blueshifted compared to $\epsilon''(\omega)$ (lower gray curve, Fig. 3(a)), owing to the frequency-dependence of $\epsilon'(\omega)$ (upper gray curve, Fig. 3(a)).

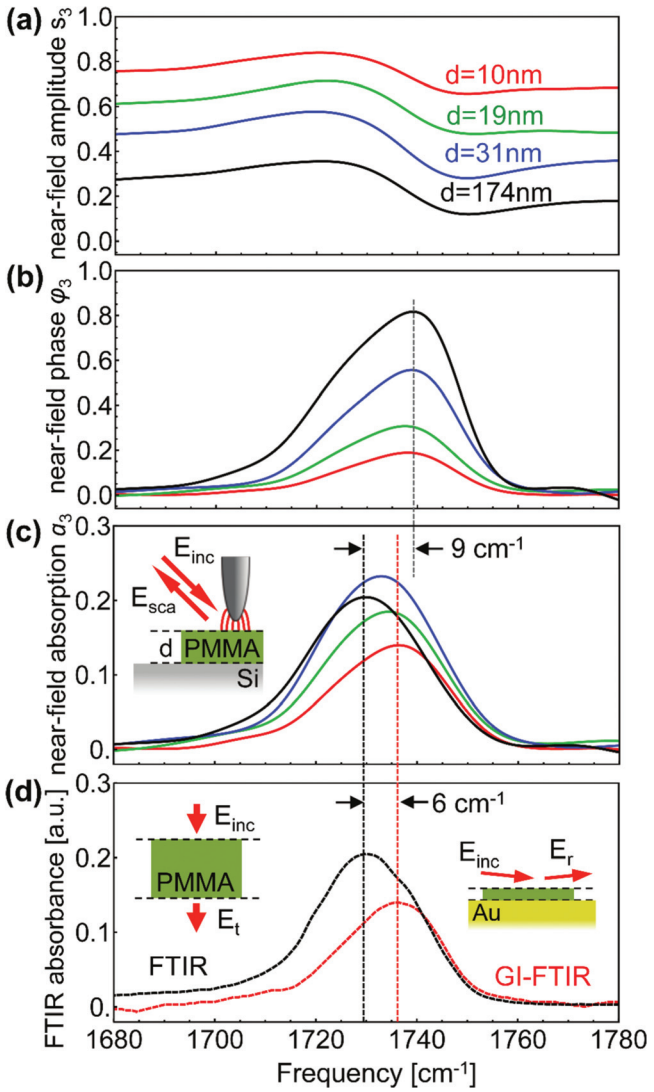

FIG. 2. Experimental spectra of PMMA. (a) nano-FTIR amplitude, (b) phase, and (c) absorption spectra of PMMA films (average of 40 interferograms, 53 min acquisition time per spectrum, 7 cm^{-1} resolution, × 60 zero filling). (d) FTIR spectrum of 1 μm thick PMMA on CaF_2 and GI-FTIR spectrum of 10 nm thin PMMA on Au substrate. Vertical black and red lines mark the peak positions.

GI-FTIR spectroscopy measures the power reflected at a thin film on a highly reflecting, typically gold covered, substrate. This power R is proportional to $|r|^2$, with r being the far-field reflection coefficient of the film-substrate system

$$r = \frac{r_{12} + r_{23}\,\exp(2ik_{z,2}d)}{1 + r_{12}r_{23}\exp(2ik_{z,2}d)}. \tag{2}$$

Here, $r_{ij} = (\epsilon_j k_{z,i} - \epsilon_i k_{z,j})/(\epsilon_j k_{z,i} + \epsilon_i k_{z,j})$ are the single-interface Fresnel reflection coefficients for p-polarized light and $k_{z,i} = (2\pi/\lambda)\sqrt{\epsilon_i - \sin^2\Theta}$. The indices $i, j = 1, 2, 3$ refer to air, film, and substrate, respectively (see Fig. 4), Θ is the angle of incidence and λ is the free-space wavelength. For simplicity, we substitute in the following ϵ_2 (the film's dielectric function) by ϵ. For optically thin films with $d \ll \lambda$, Eq. (2) can be well approximated by the two lowest orders of its Taylor expansion in $k_{z,2}d$, with the 0th-order term yielding the pure reflection from the substrate (i.e., no film) and the 1st order term describing the thickness-dependence.[22]

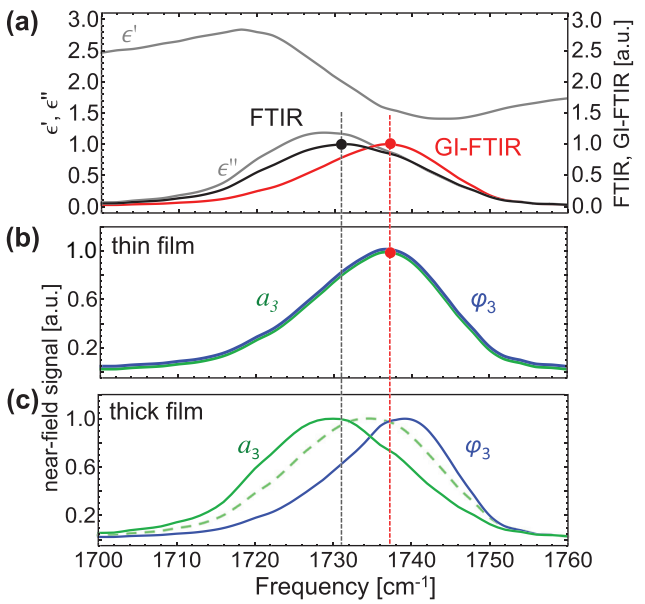

FIG. 3. Calculated spectra of PMMA (normalized to peak maximum). (a) Real and imaginary part of the dielectric permittivity of PMMA obtained by infrared ellipsometry[34,35] (gray curves). FTIR spectrum (black curve) and GI-FTIR spectrum (red curve) calculated using Eqs. (1) and (3), respectively. (b) Nano-FTIR absorption a_3 and phase φ_3 for an ultra-thin film calculated using Eq. (6). (c) Nano-FTIR absorption a_3 (green dashed) and phase φ_3 (blue) for a thick film according to Eqs. (7) and (8), respectively. Green curve is the calculation using the Finite Dipole Model (FDM),[30] which approximates the tip by an elongated, non-resonant metal spheroid. The employed model parameters are: tapping amplitude $A = 45$ nm, $R_t = 30$ nm, and the semi-major axis of the tip-spheroid $L = 300$ nm.

For highly reflective substrates ($r_{23} \approx 1$) and large grazing angles ($\Theta \sim 90°$), we obtain

$$A_r \approx 8\pi \frac{d}{\lambda}\frac{1}{\delta}\frac{1}{\epsilon'^2}\epsilon'', \tag{3}$$

where we have Taylor-expanded $k_{z,i}$ to the first order in $\delta = \sqrt{1 - \sin^2\Theta} \ll 1$ and approximated $\log(1-x) \approx -x$ for $x \ll 1$. Equation (3) explains the blueshift of the experimental GI-FTIR spectrum in Figure 2, as the prefactor $1/(\epsilon')^2$ has a much steeper slope around the resonance than the prefactor $1/\sqrt{\epsilon'}$ in Eq. (1). This blueshift can also be seen in Figure 3(a), showing the GI-FTIR (red curve) and FTIR (black curve) spectra of PMMA calculated according to Eqs. (3) and (1), respectively.

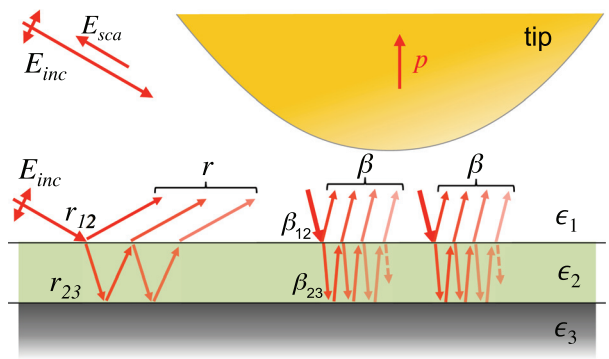

FIG. 4. Illustration of the far-field illumination of the tip, and of the near-field interaction/scattering between the tip and the sample.

For a theoretical analysis of the nano-FTIR spectra, we describe the tip-scattered field according to established s-SNOM models for non-resonant tips.[1,30] The incident field E_{inc} illuminates the tip directly and via the reflection r from the sample surface (illustrated in Fig. 4). The total field illuminating the tip, $(1+r)E_{inc}$, polarizes the tip and induces a dipole moment $p \propto (1+r)E_{inc}$, which by reciprocity, radiates back into the far field directly and via the reflection, yielding the scattered field $E_{sca} \propto (1+r)^2 E_{inc}$. In close proximity to the sample, the polarized tip interacts with the sample via the near fields localized at the tip apex. This interaction can be described as an infinite series of near-field "reflections" between tip and sample[31,32] (illustrated in Fig. 4), where the reflection at the sample surface is given by a quasi-static near-field reflection coefficient β. Limiting ourselves to a single near-field reflection from the sample, we can describe the demodulated near-field signal by $s_n \exp(\varphi_n) \propto E_{sca,n} \propto \beta(1+r)^2 E_{inc} + O(\beta^2)$. As for optically thin films $r \approx r_{sub}$,[22] the normalization to the scattering from the substrate yields the near-field contrast

$$\eta_3(\omega) \approx \frac{\beta(\omega)}{\beta_{sub}}. \tag{4}$$

For a film on a substrate, β is given by a quasistatic version of Eq. (2)[33]

$$\beta = \frac{\beta_{12} + \beta_{23}\exp(-2qd)}{1 + \beta_{12}\beta_{23}\exp(-2qd)} \tag{5}$$

with $\beta_{ij} = (\epsilon_j - \epsilon_i)/(\epsilon_j + \epsilon_i)$ and q representing the in-plane momentum of the waves scattered by the tip. While in principle the tip generates a wide spectrum of momenta q, the main contribution to the scattering comes from $q \sim 1/R_t \gg 1/\lambda$.[33] Thus, the near-field measurements can be analyzed without a rigorous integration. In the following, the two limiting cases of an ultra-thin and a thick organic film on a substrate are discussed.

For an ultra-thin film, $d \ll R_t$, on a substrate, we find $qd \sim d/R_t \ll 1$. We thus can approximate β in Eq. (5) by its Taylor expansion in qd. For highly reflective substrates with $\beta_{23} \approx 1$ (e.g., Au or Si), we can simplify the near-field contrast η_3 in Eq. (4) to $\eta_3 \approx 1 - 2qd/\epsilon$. Accordingly, we find

$$a_3 \approx \varphi_3 \approx 2qd\frac{1}{\epsilon'^2}\epsilon''. \tag{6}$$

We have neglected ϵ'' in the denominator of Eq. (6) and approximated $\arctan(x) \approx x$ for $x \ll 1$ in the derivation of φ_3.

Comparing Eq. (6) with the GI-FTIR signal in Eq. (3), we see that apart from the prefactors the expressions are virtually identical. This result explains the good experimental agreement between the near-field absorption, near-field phase, and GI-FTIR spectra of the thinnest PMMA film in Figure 2. Note that an additional linear frequency-dependence of the factor $1/\lambda \propto \omega$ in Eq. (3) is of no significant influence due to the typically small width of molecular spectral features. We corroborate our analysis by calculating the near-field absorption $a_3 = \mathrm{Im}(\eta_3)$ and phase φ_3 spectra of PMMA according to Eq. (6) (see Fig. 3(b)). The results show an excellent agreement of the nano-FTIR peak positions with the peak position of the GI-FTIR spectrum (red curve, Fig. 3(a)). We explain this agreement by the similarity of the probing mechanisms. In GI-FTIR, the probing electric field experiences reflection at the film surface and the substrate, as well as absorption in the film (reflection-absorption measurements[21]). The same reflection and absorption processes occur for the near fields when the film is thinner than the near-field decay length (compare Eqs. (2) and (5)).

The other limiting case is a thick film, $d \gg R_t$, hence $qd \sim d/R_t \gg 1$ (though still $d \ll \lambda$). Thus the exponential in Eq. (5) tends to zero, $\exp(-2qd) \to 0$, and we immediately recover the near-field absorption reported in Refs. 4 and 22

$$a_3 = \mathrm{Im}(\eta_3) \propto \mathrm{Im}(\beta_{12}) \simeq \frac{2}{(\epsilon'+1)^2}\epsilon''. \tag{7}$$

Evaluating Eq. (7) for PMMA, we observe a redshift of the near-field absorption peak (green dashed curve, Fig. 3(c)) compared to the GI-FTIR (red curve, Fig. 3(a)) and near-field phase (blue curve, Fig. 3(c)) spectra. The slight blueshift compared to the far-field absorbance spectrum of $\kappa(\omega)$ (Eq. (1), black curve, Fig. 3(a)) vanishes completely when the higher order terms neglected in Eq. (4) are considered, e.g., when the near-field contrast is calculated according to the Finite Dipole Model[30] (green curve, Fig. 3(c)). We thus confirm the experimentally observed good match between the near-field absorption a_3 and the FTIR spectrum. It can be understood by the fact that both transmission FTIR and nano-FTIR absorption of thick films are dominated by absorption in the film, with no significant far-field, respectively, near-field, reflection at the substrate.

For the near-field phase of thick organic films, we obtain

$$\varphi_3 = \arg(\eta_3) \approx \arg(\beta) \approx \frac{2}{(\epsilon')^2 - 1}\epsilon''. \tag{8}$$

The spectrum of $\varphi_3(\omega)$, calculated for PMMA according to Eq. (8) (blue curve, Fig. 3(c)), is blueshifted by about 2 cm^{-1} but comparable to the GI-FTIR spectrum (red curve, Fig. 3(a)), confirming the observations in Figure 2.

For intermediate film thicknesses, the near-field response is determined by the interplay between the thick and the ultrathin film regimes depending on the value $qd \sim d/R_t$ (Eq. (5)), giving rise to thickness-dependent peak shifts.

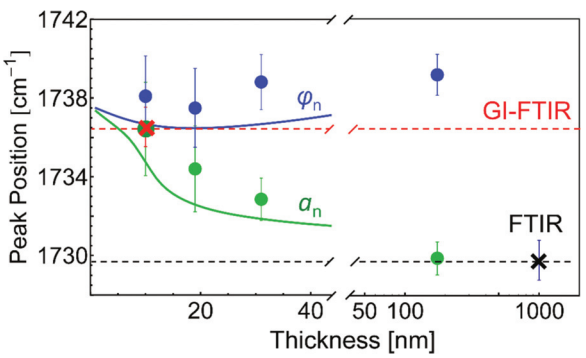

FIG. 5. Spectral peak positions as a function of PMMA film thickness. Symbols are the measured positions of the near-field phase φ_3 (blue dots), near-field absorption a_3 (green dots), GI-FTIR (red cross), and transmission FTIR (black cross) spectra. Solid lines are the calculated peak positions using the FDM-based model by Hauer *et al.*[33] with model parameters as in Figure 3.

To verify the trends observed in Figure 2, we calculated the peak positions in nano-FTIR absorption and phase spectra based on a more rigorous quasi-analytical s-SNOM model for layered samples.[33] The calculated peak position for nano-FTIR absorption (green curve, Fig. 5) quickly redshifts with increasing film thickness d, while the phase peak position (blue curve, Fig. 5) stays nearly constant. Both observations are in good agreement with the experimental results (green and blue dots, Fig. 5). The systematic blueshift of the calculation compared to the experiment is attributed to differences in the permittivity of PMMA used in experiments (495 kDa molecular weight) and in calculations (950 kDa).

Note that our results and analysis are valid only for highly reflective substrates typically employed in nano-FTIR. Calculations for weakly reflecting substrates (not presented here) indicate that the film thickness-related behavior of nano-FTIR absorption and phase spectra essentially reverse. That is, the nano-FTIR absorption peak position stays almost constant with thickness and matches well the transmission FTIR. On the other hand, the peak position of the phase spectrum is thickness-dependent: for thin films, it matches the transmission FTIR spectrum, while for thicker films it shifts towards the GI-FTIR spectrum.

In conclusion, we studied the peak positions in near-field phase φ_n and near-field absorption a_n spectra of thin organic films, both quantities related to the absorption in molecular samples. We found that the spectral position of the near-field phase is nearly constant with varying film thickness, while being blueshifted by a few wavenumbers compared to GI-FTIR spectra. When a small shift is of no major importance, near-field phase spectra promise material identification of a sample of unknown or varying thickness (size). The peak positions in near-field absorption spectra were found to agree well with that of GI-FTIR and FTIR spectra for ultra-thin and thick films, respectively, allowing for a direct comparison. When the sample thickness is intermediate or unknown, and a highly accurate measurement of an absorption feature is required, modeling is necessary to extract the absorption coefficient κ, which can be directly compared with FTIR absorbance spectra.[32] Note that our results and guidelines also apply for other amplitude- and phase-resolved s-SNOM-based spectroscopic techniques, which, for example, employ tunable laser sources.

We thank Martin Schnell (CIC nanoGUNE, Spain) for help with Synthetic Optical Holography, Roman Krutohvostovs (CIC nanoGUNE, Spain) for far-field FTIR spectra, and P. Scott Carney (University of Illinois, Urbana-Champaign) for fruitful discussions. This work was financially supported by the ERC Starting Grant No. 258461 (TERATOMO), the Department of Industry of the Basque government (ETORTEK project 2014/15), and the Spanish Ministry of Economy and Competitiveness (National Project MAT2012-36580).

R.H. is co-founder of Neaspec GmbH, a company producing scattering-type scanning near-field optical microscope systems, such as the one used in this study. The remaining authors declare no competing financial interests.

[1]F. Keilmann and R. Hillenbrand, *Nano-Optics and Near-Field Optical Microscopy*, edited by D. Richards and A. Zayats (Artech House, Boston/London, 2009).
[2]S. Amarie, T. Ganz, and F. Keilmann, Opt. Express **17**, 21794 (2009).
[3]F. Huth, M. Schnell, J. Willborn, N. Ocelic, and R. Hillenbrand, Nat. Mater. **10**, 352 (2011).
[4]F. Huth, A. A. Govyadinov, S. Amarie, W. Nuansing, F. Keilmann, and R. Hillenbrand, Nano Lett. **12**, 3973 (2012).
[5]B. Knoll and F. Keilmann, Nature **399**, 134 (1999).
[6]R. Hillenbrand, T. Taubner, and F. Keilmann, Nature **418**, 159 (2002).
[7]T. Taubner, R. Hillenbrand, and F. Keilmann, Appl. Phys. Lett. **85**, 5064 (2004).
[8]M. Brehm, T. Taubner, R. Hillenbrand, and F. Keilmann, Nano Lett. **6**, 1307 (2006).
[9]S. H. Kehr, M. Cebula, O. Mieth, T. Härtling, J. Seidel, S. Grafström, and L. M. Eng, Phys. Rev. Lett. **100**, 256403 (2008).
[10]G. Wollny, E. Bründermann, Z. Arsov, L. Quaroni, and M. Havenith, Opt. Express **16**, 7453 (2008).
[11]M. Paulite, Z. Fakhraai, I. T. S. Li, N. Gunari, A. E. Tanur, and G. C. Walker, J. Am. Chem. Soc. **133**, 7376 (2011).
[12]K. Mueller, X. Yang, M. Paulite, Z. Fakhraai, N. Gunari, and G. C. Walker, Langmuir **24**, 6946 (2008).
[13]X. G. Xu, A. E. Tanur, and G. C. Walker, J. Phys. Chem. A **117**, 3348 (2013).
[14]L. M. Zhang, G. O. Andreev, Z. Fei, A. S. McLeod, G. Dominguez, M. Thiemens, A. H. Castro-Neto, D. N. Basov, and M. M. Fogler, Phys. Rev. B **85**, 075419 (2012).
[15]S. Bergweger, D. M. Nguyen, E. A. Muller, H. A. Bechtel, T. T. Perkins, and M. B. Raschke, J. Am. Chem. Soc. **135**, 18292 (2013).
[16]In contrast to standard FTIR, the sample is located in one of the interferometer arms.
[17]I. Amenabar, S. Poly, W. Nuansing, E. H. Hubrich, A. A. Govyadinov, F. Huth, R. Krutohvostovs, L. Zhang, M. Knez, J. Heberle, A. M. Bittner, and R. Hillenbrand, Nat. Commun. **4**, 2890 (2013).
[18]P. Hermann, A. Hoehl, G. Ulrich, C. Fleischmann, A. Hermelink, B. Kästner, P. Patoka, A. Hornemann, B. Beckhoff, E. Rühl, and G. Ulm, Opt. Express **22**, 17948 (2014).
[19]X. G. Xu, M. Rang, I. M. Craig, and M. B. Raschke, J. Phys. Chem. Lett. **3**, 1836 (2012).
[20]B. Pollard, E. A. Muller, K. Hinrichs, and M. B. Raschke, Nat. Commun. **5**, 3587 (2014).
[21]P. R. Griffith and J. A. De Haseth, *Fourier Transform Infrared Spectroscopy* (Wiley, New York, 2007).
[22]A. A. Govyadinov, I. Amenabar, F. Huth, P. S. Carney, and R. Hillenbrand, J. Phys. Chem. Lett. **4**, 1526 (2013).
[23]C. Westermeier, A. Cernescu, S. Amarie, C. Liewald, F. Keilmann, and B. Nickel, Nat. Commun. **5**, 4101 (2014).
[24]A. Cvitkovic, N. Ocelic, J. Aizpurua, R. Guckenberger, and R. Hillenbrand, Phys. Rev. Lett. **97**, 060801 (2006).
[25]J. Aizpurua, T. Taubner, F. J. García de Abajo, M. Brehm, and R. Hillenbrand, Opt. Express **16**, 1529 (2008).
[26]M. Schnell, P. S. Carney, and R. Hillenbrand, Nat. Commun. **5**, 3499 (2014).
[27]While the sample is scanned, the tip-scattered radiation is superimposed at the detector with a reference wave with a linear-in-time changing phase. Recording of the detector signal pixel-by-pixel yields a synthetic hologram, in which the near-field amplitude and phase are encoded. The near-field amplitude and phase images are reconstructed by standard digital holography processing.
[28]N. Behr and M. B. Raschke, J. Phys. Chem. C **112**, 3766 (2008).
[29]J. D. Jackson, *Classical Electrodynamics* (Wiley, New York, 1999).
[30]A. Cvitkovic, N. Ocelic, and R. Hillenbrand, Opt. Express **15**, 8550 (2007).
[31]M. Esslingen and R. Vogelgesang, ACS Nano **6**, 8173 (2012).
[32]A. A. Govyadinov, S. Mastel, F. Golmar, A. Chuvilin, P. S. Carney, and R. Hillenbrand, ACS Nano **8**, 6911 (2014).
[33]B. Hauer, A. P. Engelhardt, and T. Taubner, Opt. Express **20**, 13173 (2012).
[34]Previously used in Ref. 7.
[35]A. Röseler, *Infrared Spectroscopic Ellipsometry* (Akademie Verlag, Berlin, 1990).